JOURNAL OF GEOPHYSICAL RESEARCH, VOL. 106, NO. A11, PAGES 24,611-24,620, NOVEMBER 1, 2001

Three-dimensional structuring characteristics of high-latitude plasma patches

N. A. Gondarenko and P. N. Guzdar

Institute for Plasma Research, University of Maryland, College Park, Maryland, USA

Abstract. A three-dimensional nonlinear study of the turbulence and sheared flow, generated by the gradient drift instability with ion inertial effects in the high-latitude plasma patches, is presented. Numerical simulations demonstrate quasi-two-dimensional turbulence with irregularities aligned along the magnetic field direction. Power spectra of the velocities in the plane transverse to the magnetic field and the density irregularities display anisotropy in the turbulence. Secondary Kelvin-Helmholtz instability of the gradient drift elongated vortices tends to isotropize the spectra. Ion-neutral collisions determine the level of the shear flow and therefore the saturation level of density and potential fluctuations. The irregularities penetrate through the entire patch due to the nonlinear development of the instability and do not remain localized on the edges of the plasma patch. The computed spectra and spatial structures, observed by DE 2 satellite in the midnight-noon direction, are in good agreement. The inertial terms unify the gradient drift and Kelvin-Helmholtz instabilities, the sources of small-scale structures generated in the polar cap plasma patches, and give rise to irregularity characteristics which are in a good agreement with general features of the observed structures.

1. Introduction

The high-latitude ionospheric plasma has irregularities which range over many decades of spatial scales from meters to hundreds of kilometers [*Tsunoda,* 1988; *Crowley,* 1996; *Basu and Valladares,* 1999]. The large-scale structures ranging from hundreds to thousands of kilometers have been categorized as "patches" (in the polar cap) or "blobs" (at auroral latitudes) [*Weber et al.,* 1984, 1986; *Basu et al.,* 1990, 1994]. The mesoscale features in the range of 0.1 km to tens of kilometers are believed to arise from naturally occurring instabilities in a two-component plasma. Observations [*Weber et al.,* 1986; *Basu et al.,* 1994] as well as (large-scale) modeling [*Sojka et al.,* 1993] show that the patches convect to distances of the order of 3000 km [*Weber et al.,* 1986] and for periods of a few hours while retaining their integrity. The mesoscale irregularities, observed within these patches throughout the polar cap region [*Weber et al.,* 1984, 1986; *Tsunoda,* 1988; *Basu et al.,* 1990, 1995], occasionally are more intense on the trailing edge than on the leading edge [*Weber et al.,* 1984].

In our earlier paper, three-dimensional (3-D) nonlinear simulations were presented for the collisional gradient drift instability (GDI) [*Guzdar et al.,* 1998] to model the mesoscale structures. The basic structuring occurred transverse to the direction of the magnetic field and to the direction of the ambient density gradient in long elongated "fingers". The inclusion of dynamics along the field line was responsible for slowing down the structuring process due to the stabilizing influence of parallel electric fields [*Chaturvedi and Huba,* 1987]. The structuring process for this collision-dominated (ion-neutral plasma produced a highly anisotropic spectra of the irregularities in the two directions transverse to the magnetic fields. A preliminary report of the results that demonstrated the role of the nonlinear ion inertial effects was presented by *Gondarenko and Guzdar* [1999]. It was shown that the finger-like structures developed in the early phase due to the nonlinear development of the gradient drift instability are unstable to secondary instabilities. The originally highly elongated vortices are broken up into the smaller ones because of the Kelvin-Helmholtz instability. As a result of this, the small-scale vortices can further undergo a second instability which generates shear flow transverse to the magnetic field. In this paper we discuss in detail the changes in the character of the irregularities because of the inertial terms and how the ion-neutral collisionality plays a significant role in determining both the level of the fluctuations and the nature of the turbulent spectra of the density and potential irregularities.

Paper number 2000JA000440.
0148-0227/01/2000JA000440$09.00

2. Basic Equations

The starting equations for the gradient drift instability with ion inertial effects are the continuity equation, the momentum transfer equations for electrons

and ions, and the resulting current conservation equation. The basic equations are

$$\frac{\partial n}{\partial t} + \nabla \cdot (n v_e) = 0, \tag{1}$$

$$\begin{aligned} 0 &= -\Omega_e \frac{c}{B_0}\vec{E} - \Omega_e [\vec{v_e} \times \hat{z}] - \nu_{en}\left(\vec{v_e} - \vec{V_n}\right) \\ &\quad -\nu_{ei}(\vec{v_e} - \vec{v_i}) \end{aligned} \tag{2}$$

$$\begin{aligned} \left(\frac{\partial}{\partial t} + \vec{v_i}\cdot\nabla\right)\vec{v_i} &= \Omega_i \frac{c}{B_0}\vec{E} + \Omega_i [\vec{v_i} \times \hat{z}] \\ &\quad -\nu_{in}\left(\vec{v_i} - \vec{V_n}\right) - \nu_{ie}(\vec{v_i} - \vec{v_e}) \end{aligned} \tag{3}$$

$$\nabla \cdot \vec{J} = \nabla \cdot [ne(\vec{v_i} - \vec{v_e})] = 0. \tag{4}$$

In the above, n , c, and v_q are the density, velocity of light, and velocity of species q, respectively. $\Omega_q = e_q B_0/m_q c$ ($e_q = \pm e$) is the cyclotron frequency of species q, ν_{qn} is the q species-neutral collision frequency, ν_{ei} is the electron-ion collision frequency, and $q(e,i)$ refers to electrons or ions. For the coordinate system representing the high-latitude ionosphere, the Earth's field lines are nearly vertical and assumed aligned to the z direction, the x direction is sunward, and the y direction is orthogonal to the x and z directions. A plasma patch is assumed to have a finite length along magnetic field $\vec{B} = B_0\vec{z}$ with neutral wind velocity $\vec{V_n} = V_n\vec{x}$. The electric field is $\vec{E} = -\nabla\phi$, where ϕ is the electrostatic potential.

The electron continuity and the "vorticity" equations [*Gondarenko and Guzdar,* 1999] used in our simulations were derived from (1)-(4) [*Drake et al.,* 1988]. The current conservation equation ($\nabla \cdot J = 0$), known as the vorticity equation, has contributions from differential collisional motion between ions and electrons in the direction across the magnetic field and from the parallel resistive electron motion. The normalized electron continuity and vorticity equations give rise to three dimensionless parameters, β, ν, and R [*Gondarenko and Guzdar,* 1999]. The parameter R is the ratio of the peak density $N_{\max}$ to the background density $N_{\min}$. $R = 2$ for all the simulation results presented in this paper. The density profiles are the same as those used in our earlier work as are the boundary conditions [*Guzdar et al.,* 1998].

3. Numerical Results

The evolution of the structuring of the density and potential in the nonlinear simulations of the gradient drift instability with inertial effects for the high-latitude plasma patches has been discussed previously by *Gondarenko and Guzdar* [1999]. It was shown that the initial cross-field elongated structures driven by the gradient drift instability are unstable to the Kelvin-Helmholtz instability and to the generation of sheared flows. Here we focus on the study of the changes in the scale size of the small structures generated by the secondary instability and on the effect of these changes on the isotropization of the spectra. These changes are dominantly controlled by the ion-neutral collision frequency.

The results of simulations performed with $\beta = 2000$ and $\nu = 10$ were presented earlier [*Gondarenko and Guzdar,* 1999]. There the normalization and choice of the parameters β and ν were introduced. In this work we show the results of simulations with a different value of ion-neutral collision, $\nu = 2$. Let us remind the readers that ν is the value of the ion-neutral collision frequency normalized to $1/\gamma_0 = 100$ s, so that $\nu = 2$ corresponds to the 0.02 s^{-1}. In Plates 1a-1f and 2a-2f we show the evolution of the density and potential in the xy plane near the peak of the Chapman function density profile in z at six different instances of time, t=8, 10, 12, 16, 24, and 44. The time is in normalized units, and by using normalization above one can estimate that Plates 1f and 2f correspond to 4400 s in real time. At t=8, as seen in Plate 1a, the instability starts to develop. The growth of the amplitude of the initial perturbation is caused by the gradient drift instability. At a later time, $t = 10$, the perturbation has developed to a significant amplitude so as to drastically modify the initial density profile. The potential contours at the $t = 8$ and $t = 10$ in Plates 2a-2b show the elongated vortices in the x direction caused by the primary gradient drift instability. There are ~ 25 fingers and vortices in Plates 1b and 2b, respectively. The smaller box size in the y direction (12.56 km) was specifically chosen so as to resolve these small scales. These small-scale gradient drift modes grow preferentially owing to the strong stabilizing influence of the electron dynamics along the field line of the longer-wavelength modes. Up to this point in the development of the structuring, $t \leq 10$, the spatial characteristics are very similar to that observed in our earlier work [*Guzdar et al.,* 1998] without inertia effects.

Owing to inertial effects, the extended vortices in Plate 2b, which can be viewed as shear layers, become unstable to the Kelvin-Helmholtz instability, which tends to break up these extended vortices in the x direction. This is clearly seen to happen at $t = 12$ in both the density (Plate 1c) and potential contours (Plate 2c). Now as time progresses, the irregularities evolve to larger and larger scale lengths as seen on the density contours at times $t = 16$ (Plate 1d), $t = 24$ (Plate 1e), and $t = 44$ (Plate 1f), respectively. The corresponding potential contours at t=16, 14, and 44 (Plates 2d-2f) show this transition to larger scales more clearly. This migration to a longer scale length (in the plane perpendicular to the magnetic field) is the inverse cascade process well known in two-dimensional turbulence. Even though our simulations are fully three-dimensional, the dominant convective nonlinearities are intrinsically two-dimensional in nature. It is

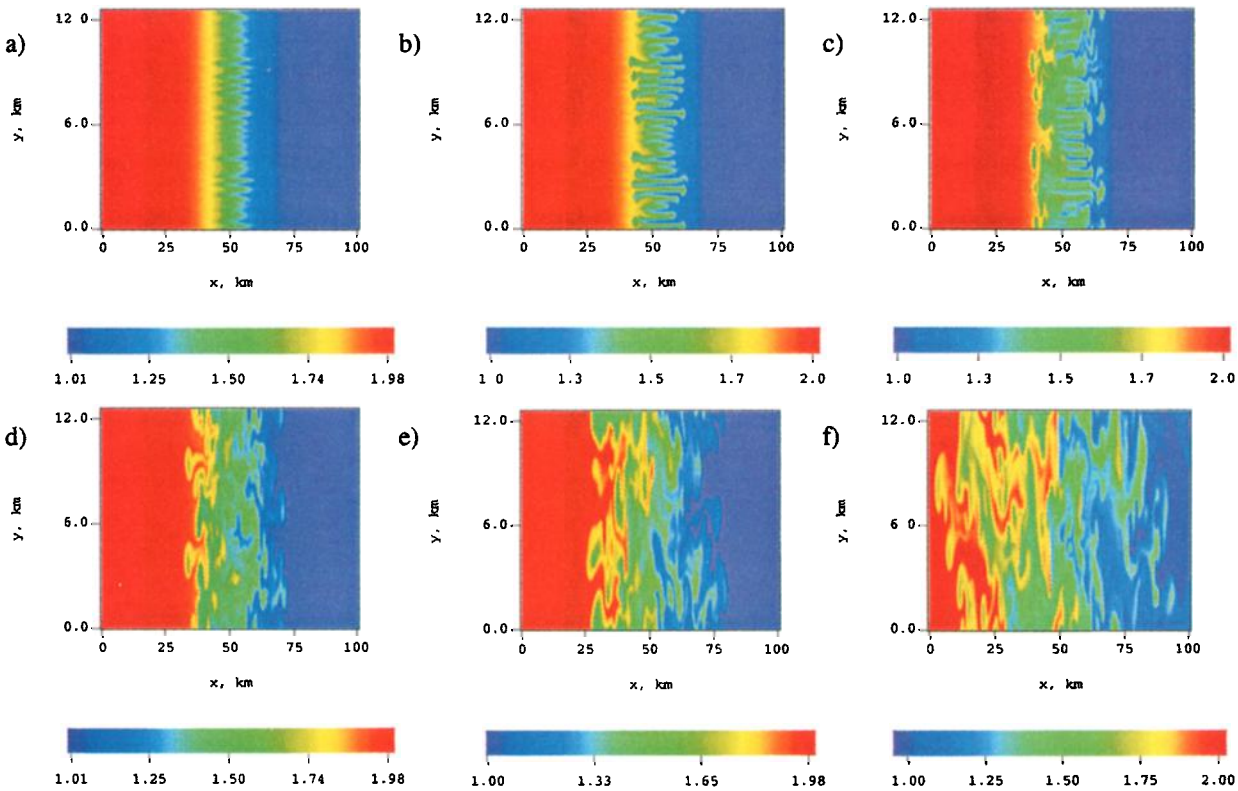

Plate 1. Density contours in the xy plane at $z = 2L_z/5$ for (a) $t = 800$ s, (b) $t = 1000$ s, (c) $t = 1200$ s, (d) $t = 1600$ s, (e) $t = 2400$ s, and (f) $t = 4400$ s. The parameters used are β=2000, $R = 2$, and $\nu = 2$.

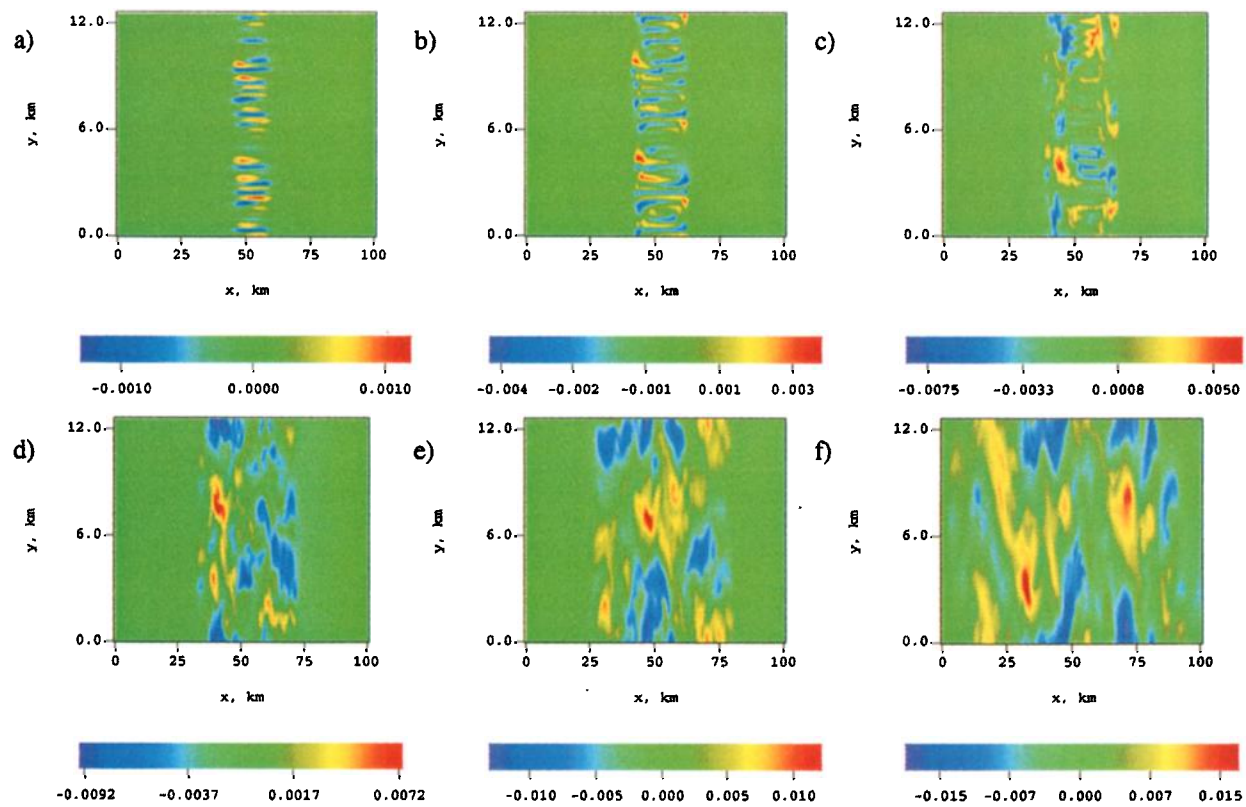

Plate 2. Potential contours in the xy plane at $z = 2L_z/5$ for (a) $t = 800$ s, (b) $t = 1000$ s, (c) $t = 1200$ s, (d) $t = 1600$ s, (e) $t = 2400$ s, and (f) $t = 4400$ s. The parameters used are β=2000, $R = 2$, and $\nu = 2$.

a)

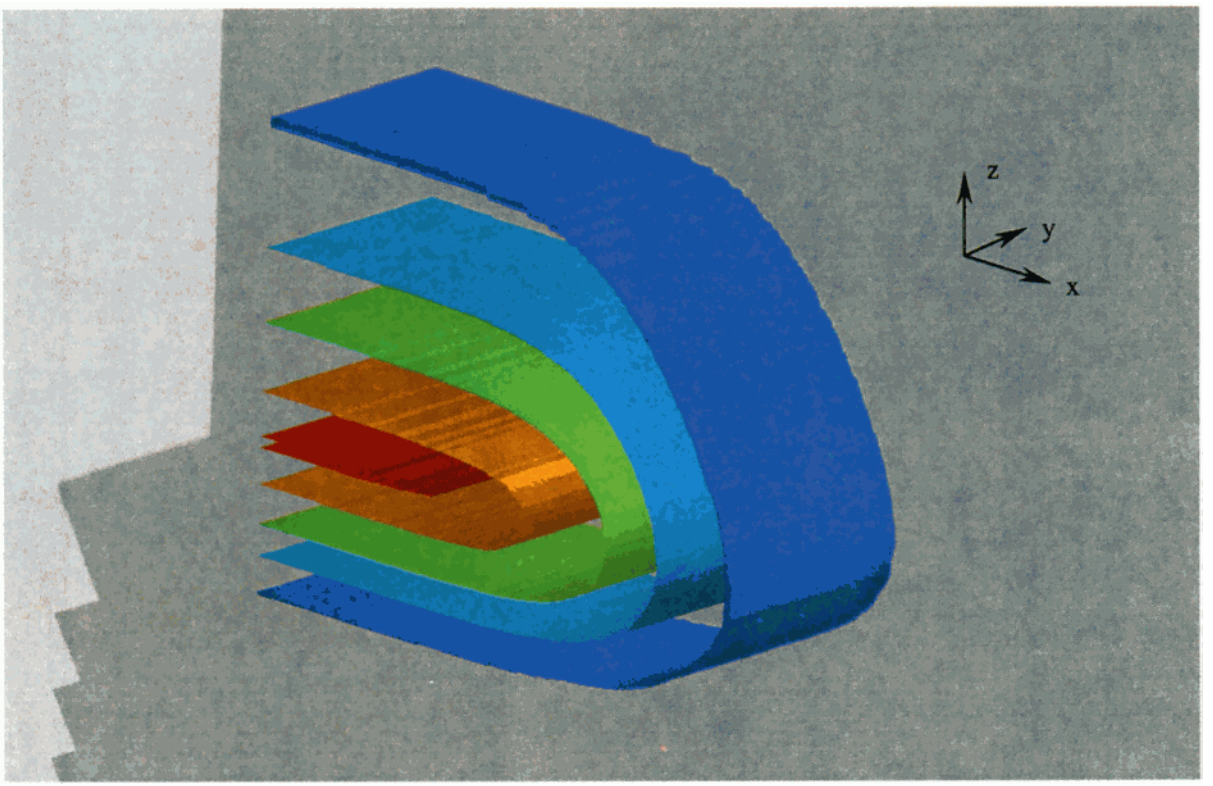

b)

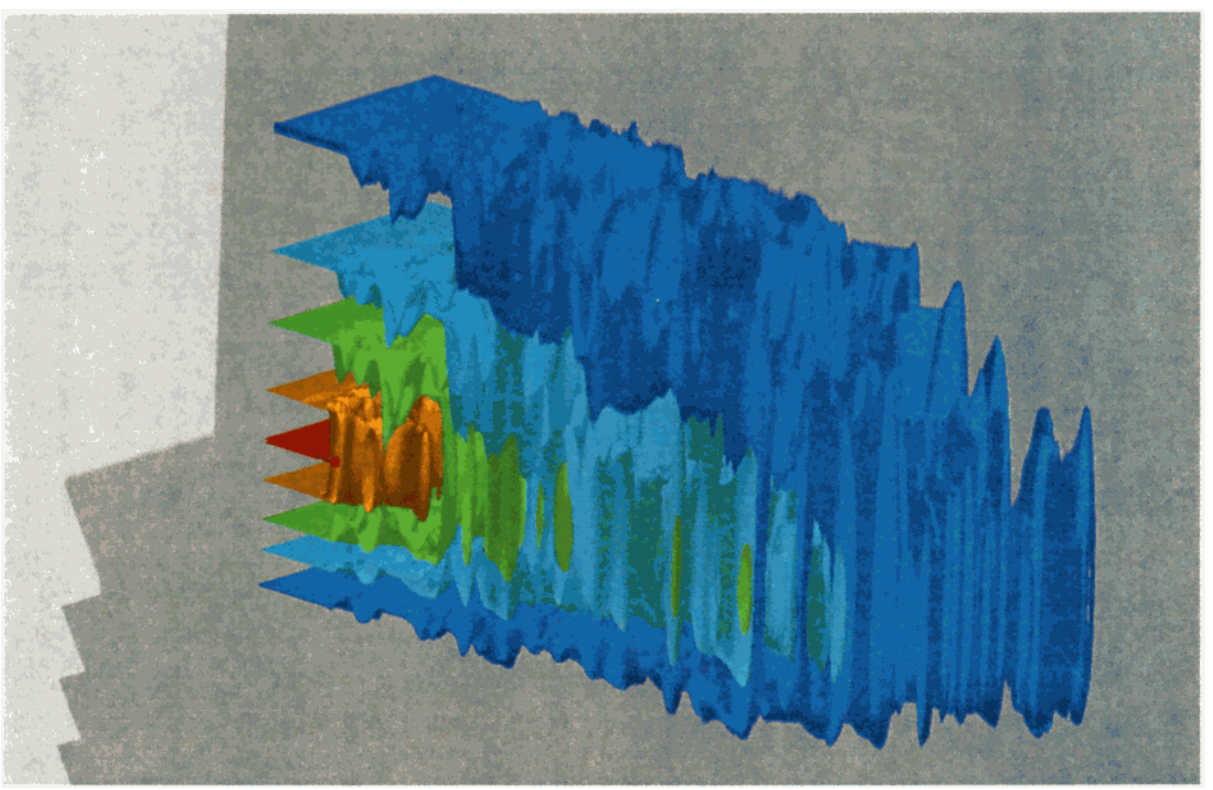

Plate 3. Five equally spaced density isosurfaces between 2 (red) and 1 (dark blue) at (a) $t = 0$ s and (b) $t = 3600$ s. The parameters used are β=2000, $R = 2$, and $\nu = 10$.

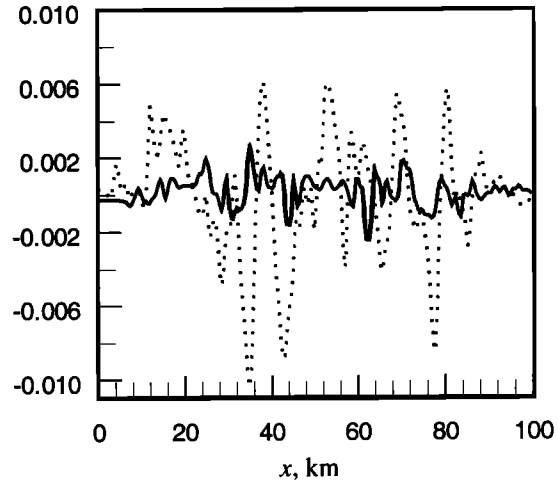

Figure 1. Average v_y velocity as a function of x for $\nu = 10$ at $t = 3600$ s (the solid line) and $\nu = 2$ at $t = 4400$ s (the dotted line). The parameters used are β=2000 and $R = 2$.

these nonlinear terms which make the turbulence quasi-two-dimensional. If we compare the results of the calculations with $\beta = 2000$ and $\nu = 2$ with the results of calculations reported by *Gondarenko and Guzdar,* [1999] (with $\beta = 2000$ and $\nu = 10$), we find that the secondary Kelvin-Helmholtz instability is stronger for the $\nu = 2$ compared to the $\nu = 10$ case. Progression of the irregularities toward the right boundary in the x direction for the present calculations with the $\nu = 2$ is slower than that with the higher ion-neutral collision $\nu = 10$. In our present simulation it took 4400 s for the irregularities to reach the right boundary, while for the calculations with the $\nu = 10$ [*Gondarenko and Guzdar,* 1999] it took $\sim$ 3600 s.

The mechanism of generation of the shear flow was discussed by *Gondarenko and Guzdar,* [1999]. It was shown that the irregularities can also generate self-consistent shear flow, and for the smaller ion-neutral collision frequency ν, the suppression of shear flow generation is reduced. The stronger generation of shear flow in the calculations with the smaller value of ion-neutral collision $\nu = 2$ compared to the $\nu = 10$ is shown in Figure 1, where the shear velocity $< v_y >$ is plotted as a function of x for the two values of the ion-neutral collision, $\nu = 10$ at $t = 36$ and $\nu = 2$ at $t = 44$. The amplitude of the $< v_y >$ for the smaller collision $\nu = 2$ is over 3 times larger than that for the $\nu = 10$ case. One observes that as the instability spreads in the x direction, multiple shear layers are produced. Shear flow provides a transport barrier, and as a consequence, it takes a longer time for the irregularities to reach the right boundary in simulations with the smaller ion-neutral collision $\nu = 2$ compared to the $\nu = 10$ case. We will return to the issue of shear flow generation later, since it plays a significant role in the saturation process for the irregularities and hence affects the magnitude of the fluctuation level of the irregularities.

In Plate 3a, five different isosurfaces equally spaced between the normalized minimum density $N_{\min} = 1$ and the maximum density $N_{\max} = 2$ initially at $t = 0$ are displayed. In Plate 3b we show the same five isosurfaces for simulation with $\nu = 10$ at $t = 36$ (which corresponds to an hour in real time). There are various interesting features associated with the structuring process. What is clearly evident is that the structuring occurs throughout the plasma patch. Since within the framework of linear theory the instability only occurs in the region where the density gradient exists, one expects that the instability, even in the nonlinear phase, will remain confined to the edges of the plasma patch. However, the nonlinear development clearly shows that

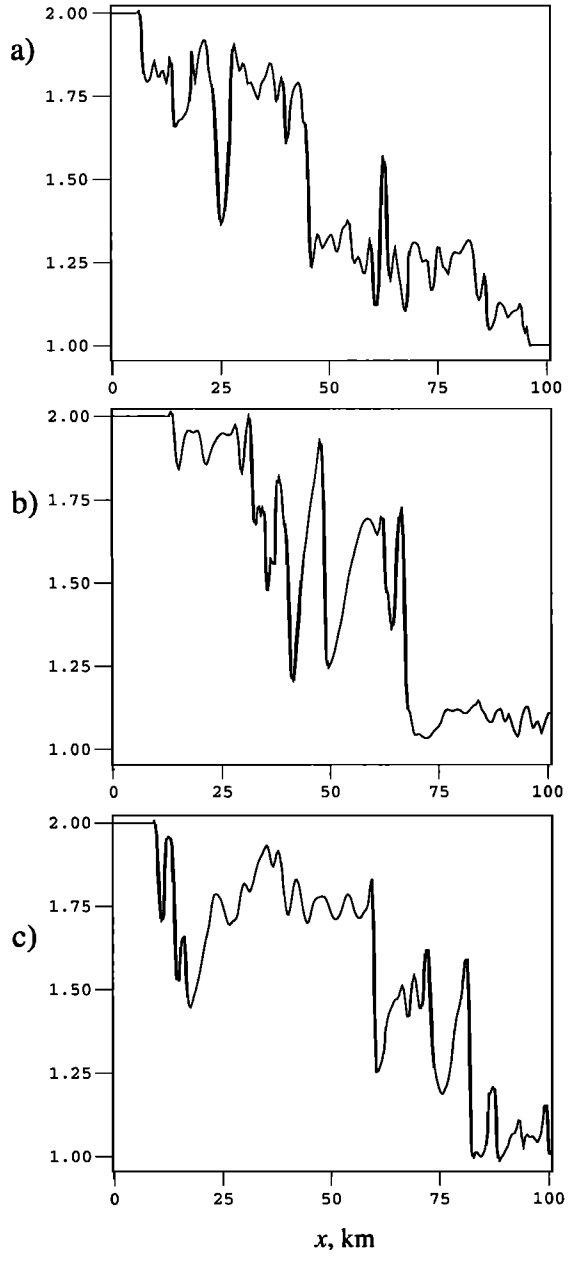

Figure 2. Density versus x at $z = 2L_z/5$ and (a) $y = L_y/4$, (b) $y = L_y/2$, and (c) $y = 3L_y/4$. The parameters used are β=2000, $R = 2$, and $\nu = 10$.

the irregularities permeate the patch and the instability develops on the nonlinearly evolving density gradient. This is also consistent with earlier simulations of the collisional Rayleigh-Taylor instability in the equatorial region, where the basic plumes were seen to extend into the linearly stable topside. Also seen very clearly in Plate 3b is that the irregularities are basically field-aligned (along the z direction). Finally, if one compares the extent of the patch along the x direction in Plates 3a and 3b, one sees that the patch has elongated in the x direction (which also is the trailing edge). This extension is due to the "anomalous" transport caused by the irregularities. The most interesting aspect of the present simulations is that even though the patch has developed significant structuring caused by a combination of the gradient drift, Kelvin-Helmholtz, and shear-flow instabilities, the patch maintains its robust characteristics. We now focus on some details of the spatial characteristics of the irregularities.

In Figures 2a-2c we display cuts at three different locations in y for the density profile in x at the peak of the density profile in z. This spatial structure would be seen by a satellite traversing the patch along the midnight-noon direction. Each realization shows that embedded in these lineouts are very steep density drops (or rises). These are associated with the edge of the "fingers" of high density as they invade the region of low density during the nonlinear development of the instability. These density lineouts are very similar to the ones reported in the work of Kivanç and Heelis [1997] as seen in their Figure 1c. The satellite pass for this particular data set was in the midnight-noon direction. The density lineout shows the same characteristics as our simulations, in which there are sharp density drops between regions of lower-amplitude irregularities. As we will discuss later, these sharp drops play a significant role in determining the spectral index of the density irregularities in midnight-noon direction.

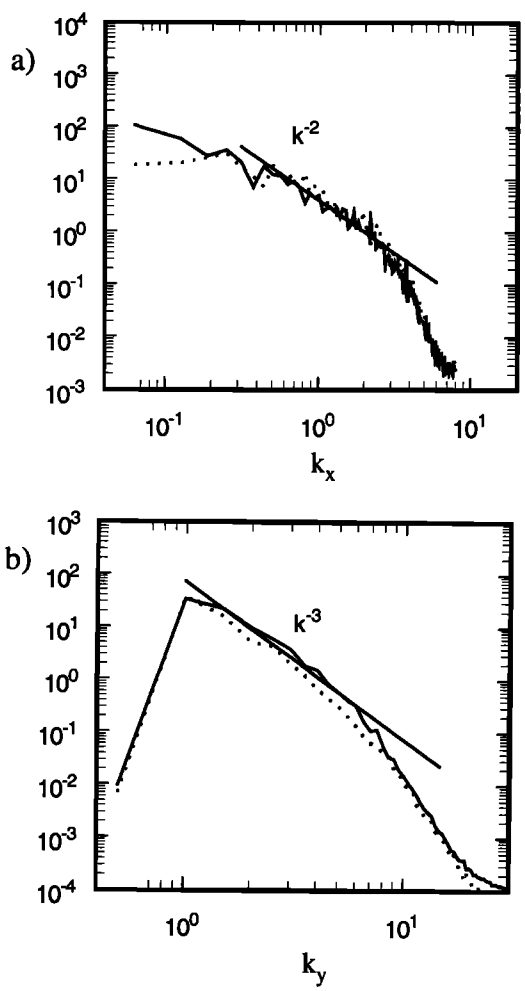

Figure 3. Density power spectra for $\nu = 10$ at $t = 3600$ s (the solid line) and $\nu = 2$ at $t = 4400$ s (the dotted line), versus (a) k_x and (b) k_y. The parameters used are β=2000 and $R = 2$.

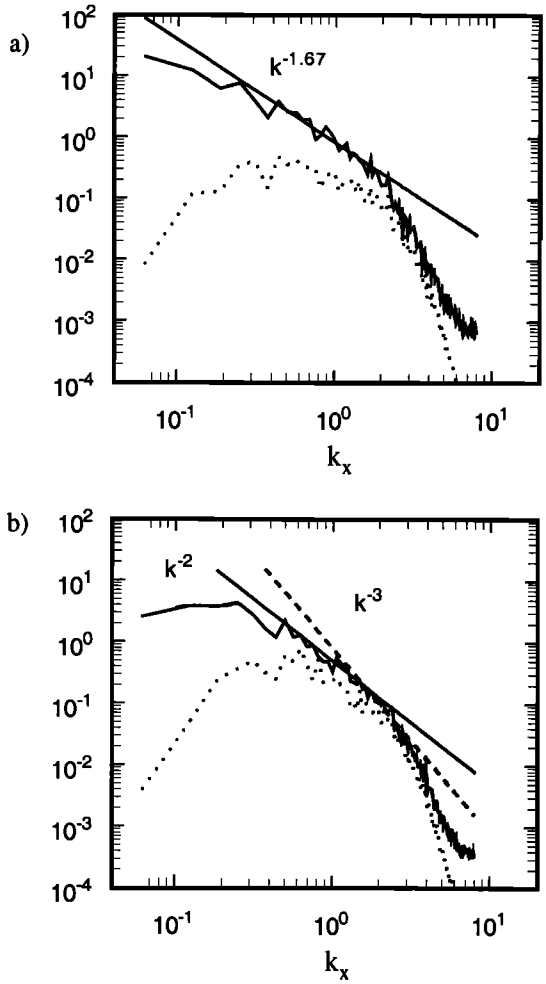

Figure 4. Power spectra of velocities v_x (the solid line) and v_y (the dotted line) versus k_x for (a) $\nu = 10$ at $t = 3600$ s and (b) $\nu = 2$ at $t = 4400$ s.

Shown in Figures 3a-3c are the spectral characteristics of the density irregularities for $\nu = 10$ and $\nu = 2$ in the midnight-noon direction x, dawn-dusk direction y, and along the field line z, respectively. It is apparent that even though the secondary Kelvin-Helmholtz tries

to isotropize the spectrum in the xy plane perpendicular to the direction of the magnetic field, there is still anisotropy in the x and y directions. One would expect to observe isotropy if the original density gradient was weak and the fluctuations were very small so that the "Boussinesq" limit was valid. However, the initial density gradient is large, and as we have seen, the fluctuation levels are in the $10-25\%$ range, hence, owing to the intrinsic difference between the x and y directions to start with, even at late time, the asymmetry is still observed. In Figure 3a, the power spectra for the density as a function of k_x for both values of the ion-neutral collisions $\nu = 10$ and $\nu = 2$ are found to fall off as ${k_x}^{-2}$ in the interval $k \in [0.5, 3]$. The long-wavelength parts of the spectra in Figure 3a are different for different values of ν. The long scales grow slower for the smaller collision ν because the stronger shear flow slows down the inverse cascade. The power law for the density power spectrum in the y direction for the $\nu = 10$ case is about -3 and even steeper for the $\nu = 2$ (Figure 3b). The approximation of the spectral indices of the power spectra for the density in k_x and k_y in the small k region shows that there is a weak anisotropy in the x and y directions. The linear lines $k^{-\alpha}$ that approximate the slope of the spectra (with α equals -2 and -3) have been added to guide the reader in looking at the longer-wavelength (smaller k) part of the spectra which are not affected by the high k hyperviscosity.

Again, if we compare the power spectrum for the density irregularities shown in Figure 3a in the midnight-noon direction with the spectrum displayed in Figure 1c in the work of Kivanç and Heelis [1997], the agreement is reasonably good. Also, the computed power spectrum for the density agrees with that reported in earlier work [*Basu et al.*, 1990]. Now we offer an explanation of the ${k_x}^{-2}$ fall-off of the density power spectrum. As shown earlier in Figure 2, there are very sharp density drops interspersed in the fluctuations. If we first obtain a linear fit to the density profile and then subtract this linear fit from the corresponding cut in Figure 2, the fluctuating density then has a series of square wave pulses associated with the sharp drops. The Fourier transform of a square pulse falls off as ${k_x}^{-1}$. Thus the power spectrum has the observed spectra index of 2.

In Figures 4a and 4b we show the power spectra for the velocities v_y and v_x as a function of k_x for $\nu = 10$ and $\nu = 2$, respectively. The power spectra for the velocity v_x in Figure 4a falls off faster compared to the fall-off of the spectrum for the velocity v_y in the interval $k \in [0.3, 2.5]$. In this interval of k space, the decrease of the amplitude of the velocity v_x can be approximated by a power law with an exponent close to 1.67. Both spectra of the velocities v_x and v_y in Figure 4a reveal anisotropy of the spectra with structures propagation in the x direction and quasiperiodical variations in the y direction. Figure 4b shows that the power spectra for the velocities v_x and v_y decrease approximately with the same power law in the interval $k \in [0.5, 3]$. At the

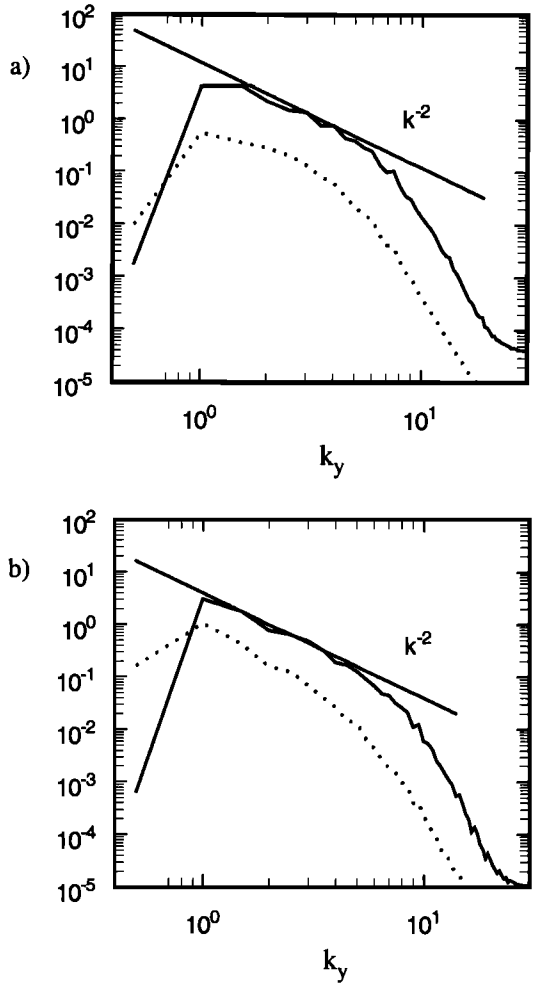

Figure 5. Power spectra of velocities v_x (the solid line) and v_y (the dotted line) versus k_y for (a) $\nu = 10$ at $t = 3600$ s and (b) $\nu = 2$ at $t = 4400$ s.

higher k, above 0.5, the amplitude of the v_y spectrum is about the same as the amplitude of the velocity v_x, indicating that the turbulence is roughly isotropic in this location. The spectral index in the region of k above 0.5 is ~ 2 and it changes to 3 at higher k. The larger spectral index in k_x for smaller ν is due to the shear flow stabilization of the high k_x modes. The spectral indices of the velocities v_x in k_x are determined by the values of the parameter ν. The spectral indices of 1.67 and 2 in k_x compare well with the spectral indices of 1.8 ± 0.2 reported from satellite measurements [*Basu et al.*, 1990; Kivanç and Heelis, 1997].

Shown in Figures 5a and 5b are the power spectra for the velocities v_x and v_y as a function of k_y for $\nu = 10$ and $\nu = 2$, respectively. The spectral index of v_x is ~ 2 for both $\nu = 10$ and $\nu = 2$ in the interval of $k \in [1, 5]$. The amplitude of the spectrum for v_x is 1 order of magnitude larger than that for v_y for $\nu = 10$. The difference in the amplitude of the v_x and v_y spectra for $\nu = 2$ in Figure 5b is smaller compared to the $\nu = 10$ case in Figure 5a. The inertial effect tries to isotropize the spectra in the xy plane (perpendicular to

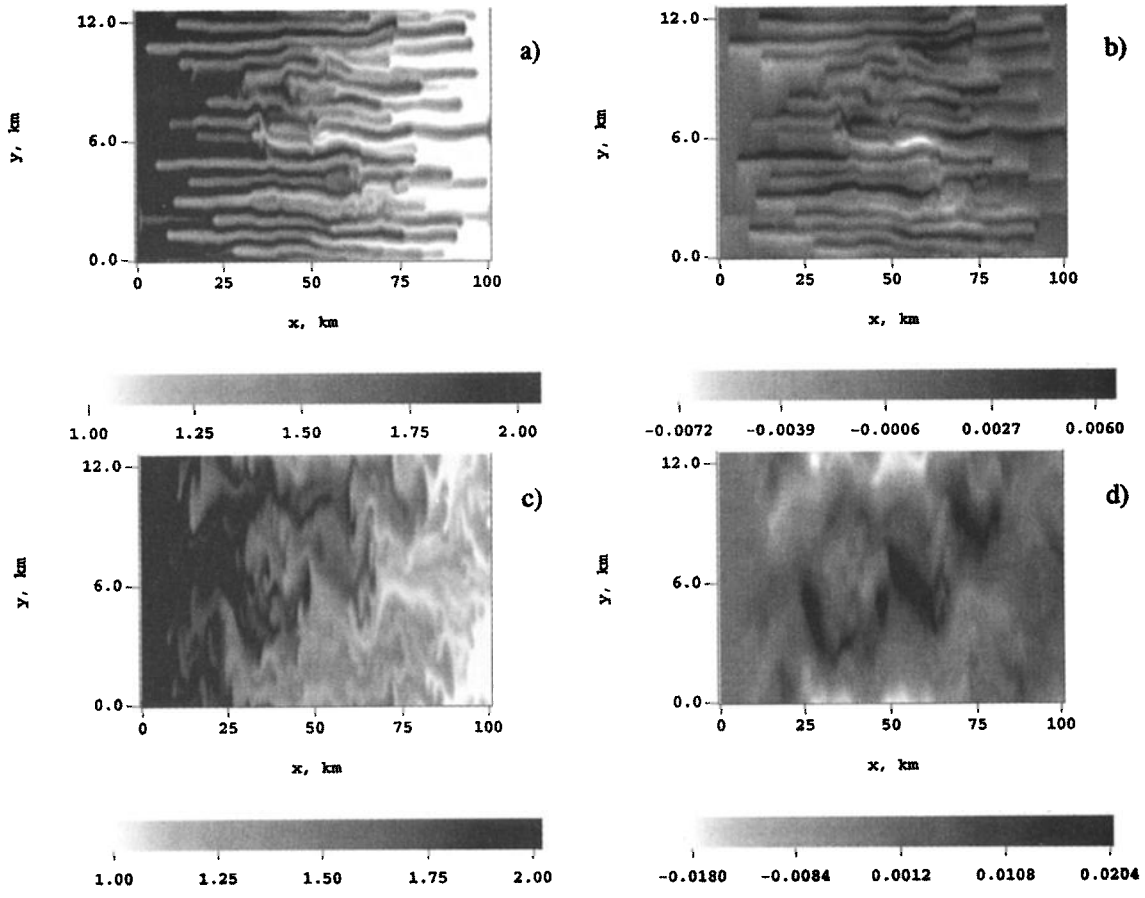

Figure 6. Contours in the xy plane at $z = 2L_z/5$ and $t = 2800$ s for $\nu = \infty$ of the (a) density and (b) potential, and at $t = 4000$ s for $\nu = 10$ of the (c) density, and (d) potential. The parameters used are β=2000 and $R = 2$.

the magnetic field), and it does so more effectively for the $\nu = 2$ case. However, complete isotropization is not possible, because of the intrinsic asymmetry between the y direction and the x direction of convection.

It is important to make more detailed comparisons of our spectra with satellite data for passes both in the midnight-noon direction and in the dawn-dusk directions. The spectra v_y and v_x in k_y for $\nu = 10$ and $\nu = 2$ shown in Figures 5a and 5b, respectively, have approximately the same spectral index equal to 2 at the long-wavelength end of the spectrum. One can notice that the slope of the power spectrum of the shear velocity v_y changes very sharply to a large value at higher k, above ~ 2.5, since the shear flow leads to a faster transfer of energy to higher k where dissipation dominates. The spectra v_y and v_x in k_x shown in Figures 4a and 4b demonstrate different behavior in the long-wavelength parts of the spectra. The v_x spectrum in k_x is dominantly the inverse cascade. The v_y spectrum cascades toward large scales more slowly.

Earlier, we had stated that the shear flow plays a significant role in determining the character and amplitude of the irregularities. In our previous work [*Gondarenko and Guzdar,* 1999] we derived an equation for the average momentum in the y direction showing that fluctuating momentum and potential can drive an average flow. That equation indicates that the ion-neutral collisions damp the shear flow. In Figures 6a and 6b are shown the structures of the density and potential irregularities in the xy plane, at the peak of the density profile in the z direction for $\nu = \infty$. Since the shear flow and Kelvin-Helmholtz (KH) are both damped by the ion-neutral collisions, the gradient drift instability generated "fingers" are not subject to the secondary instabilities. On the other hand, for $\nu = 10$, Figures 6c and 6d for the density and potential irregularities, respectively, show that the secondary KH and shear flow instabilities lead to a breakup of the fingers. Furthermore, it takes the irregularities a longer time to reach the right boundary. For the case $\nu = \infty$ the "fingers" reach the right boundary at $t = 28$, while it takes $t = 40$ for the case with $\nu = 10$.

In Figures 7a and 7b we plot the time evolution of the mean-squared density and potential fluctuation for ν=2, 10, 50, 100, and 500. Shown in Figure 7c is the RMS shear flow as a function of time for the same values of ν. It is clearly seen as expected that the magnitude of the RMS shear flow increases as ν decreases. What

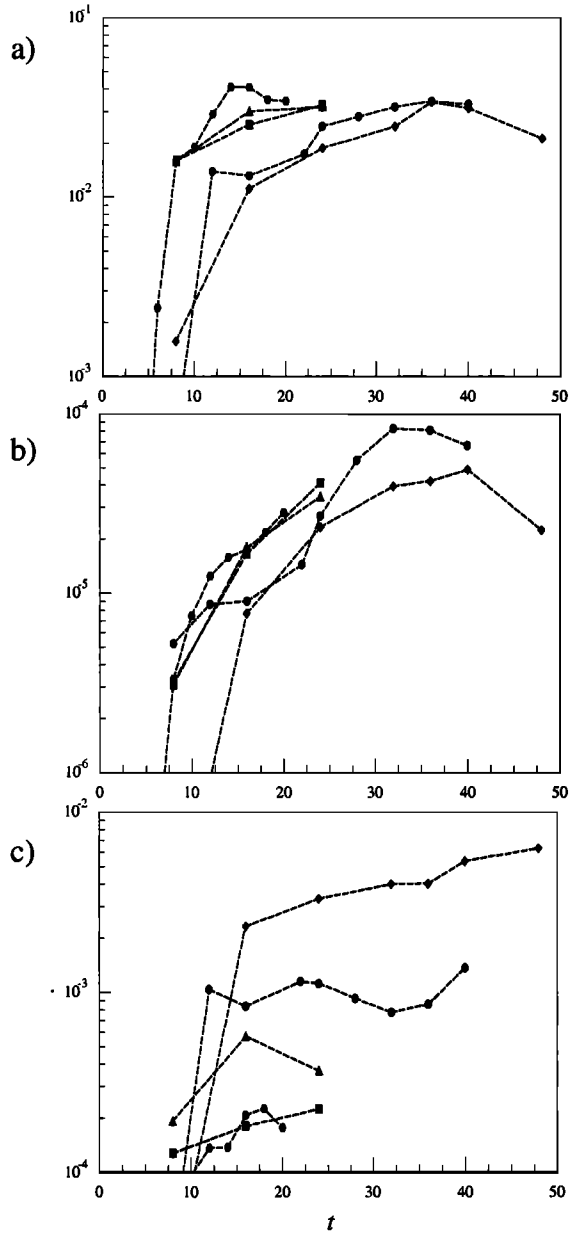

Figure 7. Time evolution of (a) mean-squared density fluctuation, (b) mean-squared potential fluctuation, and (c) the RMS shear flow v_y for $\nu = 2$ (green circle), 10 (orange circle), 50 (blue triangle), 100 (green square), and 500 (red circle).

is most interesting to observe is that the level of fluctuations decreases as the magnitude of the shear flow increases. The shear flow controls the saturation level of the fluctuations. Shear flow suppresses the irregularities. Thus the level of fluctuations and shear flow which is determined by the ion-neutral collision frequency can account for the variability observed in the patch structuring.

4. Conclusion

The presented results of our simulations demonstrate that the inertial terms combine the gradient drift and Kelvin-Helmholtz instabilities, the natural instability sources of small-scale structures in the polar cap plasma patches. Our previous results [*Gondarenko and Guzdar,* 1999] showed that Reynolds stress, the nonlinear convective part of the terms describing the inertial effects, drives the self-consistent shear flows. It was indicated that the ion-neutral collisions suppress the shear flow. In order to compare our earlier simulation results [*Gondarenko and Guzdar,* 1999] to observations [*Kivanç and Heelis,* 1998, 1997] we completed simulations with a smaller ion-neutral collision frequency ν. In the present work we show the effects of ν on the structuring characteristics of the irregularities. As the value of the ion-neutral collision is reduced, the shear flow generation and secondary Kelvin-Helmholtz instability increase. In fact, the ion-neutral collision frequency determines the level of the shear flow and therefore the saturation level of the fluctuations.

The power spectra of the density and velocities reveal the anisotropy in the turbulence. We show the temporal changes in the scale size of the vortices with evolutionary dynamics of the density and potential, revealing the inverse cascade nature of the turbulence. We have demonstrated that the Kelvin-Helmholtz instability of the original elongated vortices tends to isotropize the power spectra of the velocities in the plane transverse to the magnetic field. The results show conclusively that irregularities penetrate the entire patch because of the nonlinear development of the instability in contradiction to the linear theory notions that the instability will remain confined to the edges of the plasma patches.

Although our results show the reduction of the asymmetry in the transverse spectra since the nonlinear polarization drift generates the secondary instability of elongated vortices, it is important to make a more detailed comparison of our calculated spectra to satellite data in both directions in the plane perpendicular to the magnetic field. Our next series of investigations will focus on simulations of various scenarios with variable patch motion and also the seasonable variability in the structuring of patches by correlating it to the ion-neutral collision frequency and the initial density profile.

Acknowledgments. We acknowledge useful discussions with Sunanda Basu, Shantimay Basu, Rod Heelis, Todd Pedersen, and Jan Sojka. This research was supported by the NSF under grant ATM-9813861.

Janet G. Luhmann thanks Inez Staciarini Batista and another referee for their assistance in evaluating this paper.

References

Basu, Su., S. Basu, E. MacKenzie, W. R. Coley, J. R. Sharber, and W. R. Hoegy, Plasma structuring by the gradient-drift instability at high latitudes and comparison with velocity shear driven processes, *J. Geophys. Res.*, *95*, 7799, 1990.

Basu, S., Su. Basu, P. K. Chaturvedi, and C. M. Bryant Jr., Irregularity structures in the cusp/cleft and polar cap regions, *Radio Sci.*, *29*, 195, 1994.

Basu, S., Su. Basu, J. J. Sojka, R. W. Schunk, and E. MacKenzie, Macroscale modeling and mesoscale observations of plasma density structures in the polar cap, *Geophys. Res. Lett.*, *22*, 881, 1995.

Basu, S., and C. Valladares, Global aspects of plasma structures, *J. Atmos. Sol. Terr. Phys.*, *61*, 127, 1999.

Chaturvedi, P. K., and J. D. Huba, The interchange instability in high latitude plasma blobs, *J. Geophys. Res.*, *92*, 3357, 1987.

Crowley, G., Critical review on ionospheric patches and blobs, in *The Review of Radio Science*, p. 1, Oxford Univ. Press, New York, 1996.

Drake, J. F., M. Mulbrandon, and J. D. Huba, Three-dimensional equilibrium and stability of ionospheric plasma clouds, *Phys. Fluids*, *31*, 3412, 1988.

Gondarenko, N. A., and P. N. Guzdar, Gradient-drift instability in high-latitude plasma patches: Ion inertial effects, *Geophys. Res. Lett.*, *26*, 3345, 1999.

Guzdar, P. N., N. A. Gondarenko, P. K. Chaturvedi, and S. Basu, Three-dimensional nonlinear simulations of the gradient drift-instability in the high-latitude ionosphere, *Radio Sci.*, *33*, 1901, 1998.

Kivanç, Ö. , and R. A. Heelis, Spatial distribution of ionospheric plasma and field structures in the high latitude *F* region, *J. Geophys. Res.*, *103*, 6955, 1998.

Kivanç, Ö. , and R. A. Heelis, Structures in ionospheric number density and velocity associated with polar cap ionization patches, *J. Geophys. Res.*, *102*, 307, 1997.

Sojka, J. J., M. D. Bowline, R. W. Schunk, D. T. Decker, C. E. Valladares, R. Sheehan, D. N. Anderson, and R. A. Heelis, Modeling polar cap *F* region patches using time varying convection, *Geophys. Res. Lett.*, *20*, 1783, 1993.

Tsunoda, R. T., High-latitude *F* region irregularities: A review and synthesis, *Rev. Geophys.*, *26*, 719, 1988.

Weber, E. J., J. Buchau, J. G. Moore, J. R. Sharber, R. C. Livingston, J. D. Winningham, and B. W. Reinisch, *F* layer ionization patches in the polar cap, *J. Geophys. Res.*, *89*, 1683, 1984.

Weber, E. J., J. A. Klobuchar, J. Buchau, H. C. Carlson Jr., R. C. Livingston, O. de la Beaujardiere, M. McCready, J. G. Moore, and G. J. Bishop, Polar cap *F* layer patches: Structure and dynamics, *J. Geophys. Res.*, *91*, 12,121, 1986.

N. A. Gondarenko and P. N. Guzdar, Institute for Plasma Research, University of Maryland, College Park, MD 20742, USA. (natalia@ipr.umd.edu; guzdar@ipr.umd.edu)

(Received November 27, 2000; revised May 9, 2001; accepted May 9, 2001.)